LAWRENCE
LIVERMORE
NATIONAL
LABORATORY

UCRL-JRNL-223216

Climate Forcings and Climate Sensitivities Diagnosed from Coupled Climate Model Integrations

P. M. de F. Forster, K. E. Taylor

July 27, 2006

Journal of Climate

Updated October 14, 2003

Climate forcings and climate sensitivities diagnosed from coupled climate model integrations

Piers M. de F. Forster

School of Earth and Environment, University of Leeds, UK

and

Karl E. Taylor

Program for Climate Model Diagnosis and Intercomparison, Lawrence Livermore National Laboratory, Livermore, CA 94550, USA

Contact

Piers Forster

piers@env.leeds.ac.uk; Tel: +44 113 343 6476; Fax: +44 113 343 6716

School of Earth and Environment,

University of Leeds, Leeds, LS2 9JT, UK

Abstract

A simple technique is proposed for calculating global mean climate forcing from transient integrations of coupled Atmosphere Ocean General Circulation Models (AOGCMs). This "climate forcing" differs from the conventionally defined radiative forcing as it includes semi-direct effects that account for certain short timescale responses in the troposphere. Firstly, we calculate a climate feedback term from reported values of $2xCO_2$ radiative forcing and surface temperature time series from 70-year simulations by twenty AOGCMs. In these simulations carbon dioxide is increased by 1%/year. The derived climate feedback agrees well with values that we diagnose from equilibrium climate change experiments of slab-ocean versions of the same models. These climate feedback terms are associated with the fast, quasi-linear response of lapse rate, clouds, water vapor and albedo to global surface temperature changes. The importance of the feedbacks is gauged by their impact on the radiative fluxes at the top of the atmosphere. We find partial compensation between longwave and shortwave feedback terms that lessens the inter-model differences in the equilibrium climate sensitivity. There is also some indication that the AOGCMs overestimate the strength of the positive longwave feedback.

These feedback terms are then used to infer the shortwave and longwave time series of climate forcing in 20^{th} and 21^{st} Century simulations in the AOGCMs. We validate the technique using conventionally calculated forcing time series from four AOGCMs. In these AOGCMs the shortwave and longwave climate forcings we diagnose agree with the conventional forcing time series within ~10%. The shortwave forcing time series exhibit order of magnitude variations between the

AOGCMs, differences likely related to how both natural forcings and/or anthropogenic aerosol effects are included. There are also factor of two differences in the longwave climate forcing time series, which may indicate problems with the modeling of well-mixed-greenhouse-gas changes. The simple diagnoses we present provide an important and useful first step for understanding differences in AOGCM integrations, indicating that some of the differences in model projections can be attributed to different prescribed climate forcing, even for so-called standard climate change scenarios.

1. Introduction

With both the increase in computer power and a more complete representation of the many interactions in the climate system, climate models have become increasingly complex. Consequently, understanding their responses can often be just as difficult as understanding climate change in the real world. Radiative forcing and climate sensitivity were key concepts developed in the early days of climate modeling to aid understanding of the global mean temperature response (IPCC, 2001). These concepts remain valuable today, but forcing and climate sensitivity are more difficult to diagnose in more advanced models (Gregory *et al.*, 2004).

In this paper we propose and validate a methodology for calculating both the global mean climate forcing time series and the climate feedback in coupled Atmosphere Ocean General Circulation Model (AOGCM) simulations. We analyze recent simulations carried out in support of the Intergovernmental Panel of Climate Change (IPCC) Fourth Assessment Report. Importantly, these global time series can be calculated from routinely archived model output. To aid the understanding of inter-model differences in both 20th and 21st Century simulations, we also diagnose forcings and climate feedback terms from the current AOGCMs and provide a brief discussion of some of the more interesting findings. At each stage of our analysis, we analyze all available AOGCM output in the IPCC database.

2. Approach

The approach relies on a simple globally averaged linear forcing-feedback model. We adopt the Gregory et al., (2004) terminology, where the net flux imbalance of the climate

system (N) is related to the radiative forcing (Q), a climate feedback term (Y) and the globally averaged surface temperature change (ΔT_s)

$$N = Q - Y\Delta T_s, \qquad [1]$$

The climate feedback factor (Y) is the inverse of the climate sensitivity. As interpreted here, the equation is approximate as it only considers climate feedbacks that turn out to be proportional to global mean temperature changes (i.e., it considers the part of the energy budget from clouds, water vapor, surface albedo and lapse rate change that are proportional to global mean temperature change). These temperature changes are largely governed by the ocean mixed layer relaxation time. Therefore this equation may not accurately reflect the impact of more slowly responding aspects of climate, such as ice-sheets or the carbon-cycle.

Estimates of radiative forcing, linear global feedback, and climate sensitivity are commonly used to summarize the causes of and to quantify the reasons for climate change, as well as to predict quantitatively future climate change. Several papers, however, suggest that these simple forcing response relationships are both inaccurate and unhelpful (e.g. Boer and Yu, 2003; Aires and Rossow, 2003; and especially the critical review of Stephens, 2005). Nevertheless, we contend that a simple model remains useful, and furthermore such models provide a useful framework for more regionally-based feedback analyses, such as the linear global feedback analysis commonly used to examine and diagnose model feedback differences (e.g. Cess et al., 1996, Colman, 2003, Soden and Held, 2006, Bony et al.,2006). These papers and others provide many useful insights into cloud, water vapor and other feedbacks, and the way they are represented within climate models. Global mean radiative forcing has also been extensively used to

compare climate change mechanisms (e.g. IPCC, 2001). Even in today's sophisticated GCMs, global mean radiative forcing is a useful predictor of global mean temperature response, and forcings with very different spatial patterns can have similar patterns of surface temperature change (e.g. Forster et al, 2000; Joshi et al., 2003, Hansen et al., 2005). Reporting findings from several studies, IPCC (2001) concluded that responses to individual radiative forcings could be linearly added to gauge the global mean response, but not necessarily the regional response. Since then, studies based on both equilibrium and/or transient integrations by several different GCMs have found no evidence of important non-linearities in the global-scale climate response to changing concentrations of greenhouse gases and sulfate aerosols (Boer and Yu, 2003; Gillett *et al.,* 2004; Matthews *et al.,* 2004; Meehl *et al*., 2004). Two of these studies also examined several other forcing agents without finding evidence of a non-linear response (Meehl *et al.,* 2004; Matthews *et al.,* 2004). In all four studies, even the regional responses typically add linearly. However, some studies have found marked non-linearity for large negative solar radiative forcing (e.g. Hansen *et al.,* 2005). For the radiative forcings analyzed here, however, which are relatively small and positive, we believe a linear forcing-response assumption is justified.

Using Equation 1, Gregory *et al.* (2004) employed a simple regression technique to estimate in slab and coupled versions of the Hadley Centre GCM both the global-mean climate forcing and the climate sensitivity from experiments with *constant forcing*. Conceptually the energy balance (N) is perturbed by an initial forcing (Q); this in turn causes the climate to respond (ΔT_s), eventually returning N to zero at a new equilibrium state. Gregory *et al.* (2004) regressed N against ΔT_s to diagnose Q from the intercept and Y from the slope of the regression line. They found that the estimate of both climate

forcing (Q) and climate feedback (Y) agreed with that calculated by other methods. They also noted, however, that this "climate forcing" could be different from the conventional radiative forcing as it allowed aspects of short-term climate response in the troposphere (e.g., a semi-direct aerosol effect). As usually defined, radiative forcing does not allow the tropospheric climate state to change, but it does allow for the stratosphere to adjust (IPCC, 2001).

Forster and Gregory (2006) extended the Gregory *et al.* (2004) approach to look at transient observations of the terms in Equation 1. They specified a time series for Q and then used Equation 1 to diagnose Y from *transient* observations of N and ΔT_s during 1985-1996, when N was measured by the Earth Radiation Budget Satellite. This paper extends the same methodology one stage further. It employs Equation 1 to diagnose both Y and Q in *transient* integrations of AOGCMs. Firstly, Y values are diagnosed from integrations where CO_2 is increased by 1%/year and where the forcing due to a doubling of CO_2 concentration is known. Then these Y values are used to diagnose the climate forcing time series (Q) in both 20th Century integrations and SRESA1B (IPCC, 2000) future scenario integrations. In extending the methodology to transient integrations with changes in multiple radiative forcing agents, we make two assumptions in addition to those in Gregory *et al.* (2004): we assume that the climate sensitivity does not vary over the time-period of the integration and also that the climate sensitivity associated with multiple forcing agents is similar to that for carbon dioxide alone.

On long time-scales (~500 years), there is evidence from AOGCMs that climate sensitivity can evolve with time. To monitor the changes, an "effective" climate sensitivity has been used to describe an instantaneous climate sensitivity diagnosed from

the strengths of climate feedbacks at any point in the integration. Senior and Mitchell (2000) and Gregory et al. (2004) found in different versions of the Hadley Centre model that the effective climate sensitivity increased with time and that this was associated with the deep ocean slowly warming. In the HadCM3 the effective climate sensitivity increased after ~500 years (Gregory et al. 2004). We assume that for the ~200 year integrations described here, climate sensitivity is invariant for each AOGCM: tests described in Section 5 of this paper support this assumption.

The relative impact of various forcing agents on climate is quantified by their so-called "efficacy" -- the response of climate to a given forcing agent relative to its response to an equivalent radiative forcing of carbon dioxide (e.g. Hansen et al., 2005). Slab GCM integrations have shown that whilst different forcing mechanisms can have different efficacies (e.g. Joshi et al., 2003; Hansen et al., 2005), realistic 20th Century forcing mechanisms have efficacies within ~25% of that associated with an equivalent carbon dioxide change. Further, as the majority of the radiative forcing in the 20th and 21st Centuries was, and is expected to be, associated with carbon dioxide, the efficacy of the combined forcings over these integrations would be expected to be close to 1.0. Hansen et al. (2005) found, for example, an efficacy for combined 20th Century forcings of between 0.99 and 1.11 (depending on their evaluation methodology). For our purposes, these findings therefore justify the use of a single value for climate sensitivity.

In our analysis, the efficacy cannot be determined specifically, but instead it is incorporated into the forcing estimate (i.e., our estimate of forcing is effectively scaled by the efficacy). Likewise, because the semi-direct effect, along with stratospheric adjustment, involve feedbacks that are generally not proportional to surface temperature

response, incorporating them into the adjusted forcing, which is inferred by our method, allows one to use Equation 1 to predict future climate change more accurately. As pointed out by Shine *et al.* (2003) and Hansen *et al.* (2005), it is the effective climate forcing, after stratospheric adjustment and after accounting for various semi-direct effects and different efficacies, which is most accurate in estimating future climate responses. Imagine, for example, that the atmosphere alone (perhaps through some cloud change unrelated to any surface temperature response) quickly responds to a large *radiative forcing* to restore the flux imbalance at the top of the atmosphere, yielding a small effective *climate forcing*. In this case the ocean would never get a chance to respond to the initial *radiative forcing*, so the resulting climate response would be small and this would be consistent with our diagnosed effective *climate forcing* rather than the conventional *radiative forcing*.

3. Data

This study employs AOGCM model output obtained from the IPCC data archive (see http://www-pcmdi.llnl.gov/ipcc/about_ipcc.php). Among the variables found in this archive are monthly mean surface temperature and shortwave and longwave components of N (measured at the top of the atmosphere). As of March 2006, each model analyzed in this study had archived a preindustrial control integration, a 1%/year CO_2 increase integration, a 20th Century integration, and a SRESA1B integration. The SRESA1B integration is forced by one of the standard 21st Century scenarios for increases in greenhouse gases (IPCC, 2000). A long preindustrial control integration was run for each model. At some point part way through the control integration, the 1%/year CO_2 increase

simulation was initiated, as was the 20th Century forcing simulation[1]. The SRESA1B simulation then started from the endpoint of the 20th Century simulation. Although results from multiple simulations were available from some models, only one of the ensemble members (run 1) from each model is analyzed here[2]. In order to correct for unforced model drift, the preindustrial control simulations are run for at least 220 years beyond the time when the other scenarios began. For each model we diagnose the linear drift in N and ΔT_s from the corresponding long control simulation and this drift was subsequently subtracted from the corresponding segments of the forced integration time series. Drifts were smaller than 10% of the climate change signal in all but five of the models analyzed. Results reported here are based exclusively on global and annual averages calculated from gridded monthly mean data. Table 1 lists the models and summarizes the forcing agents included in each. Further details of the models used and the integrations can be found at http://www-pcmdi.llnl.gov/ipcc/info_for_analysts.php.

4. CO_2 radiative forcing

Although radiative forcings are not routinely calculated in coupled models, nine of the twenty models used here have submitted a calculation for the 2xCO_2 radiative forcing to the IPCC model data archive. These radiative forcings are presented in Table 2, along with the line by line model estimates of Myhre et al. 1998 (used for the IPCC, 2001 standard). Instantaneous and adjusted (i.e., after stratospheric adjustment) radiative forcings for clear skies and all-skies were calculated by the modeling groups. The average forcing from the nine models agrees very well with the line-by-line model estimate. However, there is a ~25% spread in the LW radiative forcing between models,

[1] In contrast to the other models, CCSM3, PCM, ECHO-G and MRI-CGCM2.3.2 employed a present day control integration as the starting point for its 1%/year CO_2 increase experiment.
[2] We used PCM1 upwelling tropopause flux data from run 5 for 2001-2100, as these data were not available from run 1.

and, where included, models have very different SW radiative forcings. Also bear in mind that the other modeling groups have not recorded radiative forcings, so the twenty model spread could be larger still.

IPCC (2001) and Myhre et al. (1998) give a simple, but accurate, formula for the radiative forcing from CO_2 changes of $Q_{CO2}(NET) = 5.35.\ln(C/C_o)$, where C_o is the unperturbed concentration and C the perturbed concentration of CO_2. This formula gives the $2xCO_2$ radiative forcing value shown in Table 2. We use the SW and LW split of the $2xCO_2$ NET forcing from Myhre et al. (1998) (Table 2) with this simple formula to obtain LW and SW time series of radiative forcing for a 1%/year CO_2 increase. Thus, the model radiative forcing timeseries are represented by

$Q_{CO2}(LW) = f.year.5.57.\ln(1.01)$; $Q_{CO2}(SW) = f.year.-0.22.\ln(1.01)$,

where *year* is the number of years since the start of the integration (up to 70 years, the time of CO_2 doubling) and *f* is the ratio of the models' $2xCO_2$ radiative forcing estimate to the IPCC/Myhre et al. (1998) value. Many models continued their integration for an additional 150 years, keeping CO_2 constant after year 70. For models that did not record their $2xCO_2$ radiative forcing, time series were generated assuming f=1.

5. Climate Sensitivities

Twenty AOGCMs provided flux and temperature data from their 1%/year CO_2 increase integration, allowing us to calculate the feedback strength, as gauged by *Y*. After the drift in the control climate integration was subtracted from the 1%/year CO_2 integration, the first 70 years of the *N* and ΔT_s time series were calculated as the difference from the beginning of the runs. With Equation 1 applied separately to the shortwave and longwave

components of radiation, values of Y and their statistical uncertainty are calculated, based on the Q time series from Section 4, by regressing Q-N against ΔT_s (Figure 1 and Table 3). Ordinary least squares (OLS) regression is used. The autocorrelations in the Q-N time series were high. Lag 1 correlations were typically 0.9 in the LW and 0.8 in the SW. These autocorrelations are accounted for when evaluating the statistical uncertainties. Forster and Gregory (2006) give extensive justification for the use of OLS regression within this climate modeling framework. Their argument is based on the reasoning that ΔT_s is the likely driver for most of the changes in N. In practice the choice of regression model made little difference to the overall results, especially in the longwave.

Figure 1 shows the results for the two models that had the best and the worst fits to Y. All the models began their 1%/year integration close to equilibrium (the origin on the graph). The derived Y values and their uncertainties are shown for all models in Table 3. Most models had a very good straight-line fit to Y-LW, as illustrated by CGCM3.1(T47) (Figure 1). Likewise, the Y-NET value had small statistical uncertainties (Figure 1 and Table 3). Importantly, no model obviously departed from a straight line fit: i.e. Y appears constant over these 70 years.

Even when the complete 220 year integration was included in the analysis, most models still exhibited a constant Y-LW. Exceptions are shown in Figure 2, where three models clearly exhibit temporal variation in Y-LW. Data after 70 years were not available from the Hadley Centre, therefore we were unable to test the non-linearities previously found with its models (see Section 2). The GFDL-CM2.0 model has a response very similar to GFDL-CM2.1. In the CNRM-CM3 model the slope changes after 70 years, which likely indicates that the specified forcing could be in error: we found that reducing the LW

forcing by 10% improved the straight line fit. Only the GISS-EH model shows a large departure from a constant value for Y-LW. Interestingly, the GISS-ER model (not shown) does not exhibit this non-linearity. As there is no noticeable change in gradient after 70 years and the $2xCO_2$ forcing is known (see Table 2), errors in forcing are unlikely to be the cause. The variation in Y could be explained if the model's ocean did not start near quasi-equilibrium at the beginning of the integration and was undergoing significant adjustment over the analysis period (see Senior and Mitchell, 2000). Analysis of global mean temperature trends in the pre-industrial control integrations supports this theory. Over a 200 year period the global mean surface temperature in the GISS E-H model's control integration cools by about 1K, whilst the GISS E-R model's surface temperature does not have a trend.

For a further check of our results we compare the diagnosed Y-NET values given in Table 3 to values computed from actual equilibrium experiments from a slab version of the corresponding model. The global mean equilibrium surface temperature changes for 11 models were available. From the time series generated by each of these models, we selected years following the initial transient warming phase. The time series of annually and globally averaged surface temperature was plotted and the post "transient warming" years were identified by visual inspection. Then for those selected equilibrium periods, we calculated the difference between the multi-year mean for the control and $2xCO_2$ runs, yielding the equilibrium temperature change. The NET radiative forcing from Section 4 is then divided by these temperature changes, to obtain the Y-NET($2xCO_2$) values that are shown in Table 3. Within the quoted statistical uncertainty there is an approximate correspondence between these equilibrium Y-NET($2xCO_2$) values and the diagnosed Y-NET values in the table. Agreement would not be expected to be perfect, as the presence

of an ocean model could readily modify the atmospheric feedbacks (Gregory *et al.*, 2004).

Figure 3 graphically illustrates the range of derived *Y* values (from the 70-year integrations) and their uncertainties. The Figure compares Y values to the uncertain estimate from Earth Radiation Budget observations made in Forster and Gregory (2006). In the models, the range of Y-LW and Y-NET values is less than a factor of two. Also, these values are always smaller than 3.3 $Wm^{-2}K^{-1}$, the value of *Y* for a black-body response (sometimes referred to as the Stefan-Boltzmann radiative damping). This indicates a positive LW feedback. For some models their large positive longwave feedback (smaller positive Y-LW) does not appear consistent with the Y-LW found from the observationally-based estimate (Figure 3). Forster and Gregory (2006) note that the sign of the observationally-based estimate of longwave cloud feedback is negative, in disagreement with most models, but the *Y* values derived from the observations are very uncertain.

For all models, shortwave feedback is positive (i.e., Y-SW is negative). These values, however, are less constrained by the regression than the LW values, and for a few models the statistical uncertainties are too large to constrain the sign (Figures 1, 2, 3 and Table 3). Forster and Gregory (2006) also noted similar difficulties in constraining Y-SW. Interestingly, there is some compensation between Y-SW and Y–LW, i.e. those models with the largest positive shortwave feedback also have the smallest positive longwave feedback (Figure 3, Table 3). This may be attributable to differing strengths of their cloud amount feedback. In most models cloud fraction decreases as surface temperatures rise, this leads to a positive shortwave cloud feedback and negative longwave cloud feedback

(Cess *et al.*, 1996; Bony *et al*., 2005). The 2xCO_2 equilibrium *Y* range (Figure 3 and Table 3) is similar to that from the range of model sensitivities quoted in IPCC (2001).

The regression technique we use to derive *Y* values works considerably better here than it did for the constant forcing experiments in Gregory *et al.* (2004). In their experiments, *N* approached equilibrium so rapidly that only a few data points were available to constrain the statistics of the regression line. In the 1%/year CO_2 increase transient integrations of this paper, the *Y* values are much better constrained. There is also no evidence of a change in *Y* values over the 70 year time period of the CO_2 increase, and most models had no evidence of a change in *Y* over all 200+ years of the integration. These findings suggest that in most AOGCMs our simple forcing response concepts are still applicable. However, as long-term data were not available from the Hadley Centre models to evaluate Y values after 70 years and the GISS E-H model exhibited a significant non-linear response, caution needs to be used when assuming an invariant Y, as we do in Section 6 of this paper.

6. Derived Climate Forcings

In the final part of this paper we combine the *N* and ΔT_s values from the 20th and 21st Century integrations (~1880-2100) with the *Y* values already diagnosed in Section 5 to find the time series of climate forcings, presented in Figures 4 and 5. The models from Section 5 contributed flux and temperature data for both a 20th Century integration and an SRESA1B integration. Using these data, LW and SW components of the climate forcing (Q) are derived separately from Equation 1. The total SW forcing includes a component due to any changes in the solar constant. This solar forcing is shown as the blue lines on the figures, as it can be diagnosed directly from changes in the models' downward

shortwave flux at the top of the atmosphere. For comparison, the figure also shows the radiative forcing time series for the 20th Century from Myhre et al (2001) and for the 21st Century SRESA1B scenario from IPCC(2001, Appendix 2). A summary of the climate forcing changes over 50 and 100 year intervals is shown in Figure 6, and Table 3 shows, relative to the preindustrial control, the total climate forcing and surface temperature change up to year 2100.

The climate forcing time series we derive are contaminated by changes in *N* that are unrelated to surface temperature change. These fluctuations are largest in the shortwave and in the models where the same variations in *N* contributed most to the uncertainty in *Y*. Their effect on the forcing time series can clearly be seen in the unsmoothed data presented in Figure 4. They appear to be of a small enough magnitude and occur over a sufficiently short timescale not to mask the major features of the time series. The diagnosed SW and LW climate forcing time series for the 20th Century have been verified for the two modeling groups (four models) that were able to provide time series of radiative forcings used in their model simulation; these were produced by off-line radiative transfer codes and are shown as magenta lines on Figure 4 for the MIROC models (Toshihiko Takemura, pers. comm.) and the GISS models (James Hansen, pers. comm.). These radiative forcings were provided as individual time series for each major forcing agent and these time series were then combined to obtain estimates of total shortwave and longwave radiative forcings. The reported well mixed greenhouse gas forcing was assumed to be longwave only and the reported aerosol and solar forcings were assumed to be shortwave only; ozone and volcanism were taken to be composed of shortwave and longwave components which are estimated using the reported net forcing, partitioned according to IPCC (2001, Chapter 6). Figure 4 shows that the groups' forcing

estimates agree very well with that diagnosed using our simple methodology. For the GISS models there is a small discrepancy (~10%) between our diagnosed forcing estimate and the radiative forcing provided by the GISS group. Given that Hansen *et al.* (2005) found a 20th Century efficacy close to 1.0 with the same model, the difference is unlikely to be due to an efficacy effect.

By inspecting the shortwave and solar forcing results for the 20th Century, it is easy to identify the models that include natural forcings in their integrations (also see Table 1). Solar forcings are directly diagnosed from the downward solar flux, and the volcanic forcing manifests itself as a series of negative spikes. The solar and volcanic forcing signals are similar in size and shape in most models that incorporate them (Figure 4 and Table 1). However, the volcanic forcing is too small in the MRI-CGCM2.3.2 model, which incorporates it as a change in the solar constant. Several models have a negative total shortwave forcing, presumably due to scattering by tropospheric aerosols (see Table 1). The strength of this aerosol effect differs greatly between the models and some, such as the two GFDL and CCSM3 models, do not appear to have a significant NET tropospheric SW forcing (Figure 4); this is likely due to a cancellation effect between scattering sulfate aerosols and absorbing black carbon aerosols, as both types are included in these models (see Table 1). Overall these differences in included SW forcing agents described in Table 1 (e.g. aerosols, solar and volcanic effects) lead to a wide range in the shortwave forcings for the 20th Century (Figure 6).

Compared to the range of shortwave forcings, the longwave forcings for the 20th Century are in better agreement with each other and are similar to the estimates of Myhre *et al.* (2001). The shapes of the different longwave Q time series are similar (Figure 4), but the

magnitude of the estimated forcing still differs by a factor of two; compare, for example, the range of LW climate forcings shown in the top three panels of Figure 6.

For the 21st Century (Figure 5) there is a much wider spread in the range of climate forcing estimates. Most models have an increasing SW climate forcing, presumably due to tropospheric aerosol reductions. The GISS models, however, have clear negative forcing trends which would partly offset the effect of their larger-than-average LW forcing. In the LW, the spread of the 2000-2100 climate forcing estimate is a factor of two. There is also some inconsistency in the time-evolution of 21st Century longwave forcing changes (Figure 5)). Particularly apparent is the relatively small increase in LW forcing in the latter part of the 21st Century for the GFDL-CM2.1, IPSL-CM4, NCAR-PCM1 and MRI-CGCM2.3.2 models; reasons for this remain undiscovered.

The range of model forcing estimates illustrated in Figures 4, 5, and 6 is perhaps surprising given that most of the LW forcing would be expected to be due to carbon dioxide, and the LW carbon dioxide forcings agreed to within 25% for the models evaluated (Table 2 and Section 4). Forcings from other well-mixed greenhouse gases and ozone would, however, also affect these time series. Further, several models that did not evaluate their CO_2 forcing are outliers on Figure 6, thus the actual spread in model CO_2 forcing could be greater than indicated by Table 1. Among 16 GCM radiation codes employing identically prescribed clear-sky vertical atmospheric profiles of temperature and water vapor, Collins et al. (2006) find spreads of up to 40% in their carbon dioxide forcing and 60% in their well-mixed-greenhouse gas forcing.

7. Conclusions

This paper has introduced a simple way of retrieving global mean climate forcing from energy balance and surface temperature diagnostics in coupled climate models. This is done by firstly estimating a global climate feedback term from integrations where CO_2 is increased by 1%/year. Then the climate feedback term is used to diagnose climate forcing time series in transient climate change experiments with unknown radiative forcings.

This methodology can be applied as a useful first step to aid understanding of AOGCM differences. Forcings are not routinely calculated by models, but without knowing them differences in model response are hard to interpret. Our results provide several useful illustrations of this. Three examples are discussed below.

Firstly, one might assume that, as all models followed the SRESA1B scenario, differences in model response would be more likely due to climate response, rather than forcing. Our results in Table 3 suggest, however, that forcing scenarios also account for a significant fraction of the differences in temperature change found at year 2100: the models with the smallest NET forcing in 2100 also tend to be the ones with the smallest surface temperature change. Secondly, comparison of the responses in two versions of the MIROC model leads to the unexpected result that at the end of the 21st Century, the larger temperature change found in the 'hires' model could be due to a stronger LW climate forcing, rather than a different climate response. Inspection of the Y-NET and Q-NET values in Table 3 supports this conclusion. Thirdly, the technique also helps evaluate a single AOGCM's forcing, which, for example, enabled us to determine that the volcanic forcing in MRI-CGCM2.3.2 is too small compared to previously published volcanic forcing estimates (see Section 5).

Importantly, our paper suggests that several AOGCMs may not correctly model the forcing from well-mixed-greenhouse-gases. We found, across models, a large range in LW forcing and different time-evolution of this forcing, which is surprising given that greenhouse gas changes should account for most of this forcing and that this forcing should be essentially the same in every model. These results support the findings of Collins et al. (2006) and suggest that in AOGCMs the radiative transfer of the well-mixed greenhouse gases should be examined as a matter of some urgency.

The diagnosed forcings are not designed to replace conventional radiative forcing calculations. The diagnosed climate forcings cannot be split into components associated with different forcing agents (unless multiple integrations with individual forcing agents are performed), nor can it diagnose spatial patterns of forcings, so our analysis is somewhat limited if a more detailed understanding of climate forcing and response is sought. The techniques themselves also employ several assumptions that are not necessarily always valid. These assumptions (see Sections 5 and 6 for details) would suggest that the techniques are only likely to work well in ~100 year integrations that are slowly warming, largely as a response to CO_2 increases. Further, although the technique gives good results in current AOGCMs, the linear forcing response model may not be valid in future AOGCMs that will likely incorporate additional climate feedbacks, such as biogeochemical effects.

Despite these caveats it is hoped that the simple methodology presented in this paper will be routinely applied to diagnose coupled model integrations. Knowing the global climate forcing should be a first step in the quest to understand both an individual model's response and differences between models. Comparing this climate forcing diagnostic to

conventionally calculated radiative forcing would also provide a useful estimate of the semi-direct effect.

Acknowledgements

Toshihiko Takemura and Jim Hansen are thanked for providing radiative forcing data, and we thank Ben Santer for carefully compiling the information used in Table 1. Jonathan Gregory and Jim Haywood are thanked for helpful discussion of the ideas used in this paper. We also appreciate the helpful suggestions made by two anonymous reviewers. We gratefully acknowledge the international modeling groups for providing their data for analysis, the Program for Climate Model Diagnosis and Intercomparison (PCMDI) for collecting and archiving the model data, the JSC/CLIVAR Working Group on Coupled Modeling (WGCM) and their Coupled Model Intercomparison Project (CMIP) and Climate Simulation Panel for organizing the model data analysis activity, and the IPCC WG1 TSU for technical support. The IPCC data archive and work at the University of California, Lawrence Livermore National Laboratory is supported under the auspices of the U.S. Department of Energy Office of Science (Climate Change Prediction Program) under contract No. W-7405-ENG-48.

References

Aires, F., and W.B. Rossow, 2003: Inferring instantaneous, multi-variate and non-linear sensitivities for the analysis of feedback processes in a dynamical system: The Lorenz model case study. *Q. J. Roy. Meteor. Soc.*, **129**, 239-275.

Boer, G.J., and B. Yu, 2003: Climate sensitivity and response. *Clim. Dyn.,* **20**, 415-429.

Bony, S., R. Colman, V. Kattsov, R. P. Allan, C. S. Bretherton, J.-L. Dufresne, A. Hall, S. Hallegatte, M. M. Holland, W. Ingram, D. A. Randall, B. J. Soden, G. Tselioudis, and M. J. Webb, 2006: How well do we understand climate change feedback processes? *J. Clim*., in press.

Cess, R.D., V. Alekseev, V. Dymnikov, V. Galin, E.M. Volodin, H.W. Barker, M.H. Zhang, E. CohenSolal, H. LeTreut, R.A. Colman, J.R. Fraser, B.J. McAvaney, D.A. Dazlich, L.D. Fowler, D.A. Randall, A.D. DelGenio, K.K.W. Lo, M.R. Dix, M. Esch, E. Roeckner, W.L. Gates, G.L. Potter, K.E. Taylor, J.J. Hack, W.J. Ingram, J.T. Kiehl, J.F. Royer, B. Timbal, V.P. Meleshko, P.V. Sporyshev, J.J. Morcrette, M.E. Schlesinger, W. Wang, and R.T. Wetherald, 1996: Cloud feedback in atmospheric general circulation models: An update. *Journal of Geophysical Research-Atmospheres,* **101**(D8), 12791-12794.

Collins, W.D., V. Ramaswamy, M.D. Schwarzkopf, Y. Sun, R.W. Portmann, Q. Fu, S.E.B. Casanova, J.-L. Defresne, D.W. Fillmore, P.M.D. Forster, V.Y. Galin, L.K. Gohar, W.J. Ingram, D.P. Kratz, M.-P. Lefebvre, J. Li, P. Marquet, V. Oinas, T. Tsushima, T.

Uchiyama, and W.Y. Zhong, 2006: Radiative forcing by well-mixed greenhouse gases: Estimates from climate models in the IPCC AR4. *J. Geophys. Res.,* in press.

Colman, R.A., 2003: A comparison of climate feedbacks in general circulation models, *Clim. Dynam.*, 20, 865–873.

Forster, P.M., and J.M. Gregory, 2006: Diagnosing the climate sensitivity and its components from Earth Radiation Budget Data. *Journal of Climate,* **19,** 39-52.

Forster, P. M. de F., Blackburn, M., Glover, R. and K. P. Shine, 2000: An examination of climate sensitivity for idealized climate change experiments in an intermediate general circulation model, *Clim. Dynam.*, **16**, 833-849.

Gillett, N.P., M.F. Wehner, S.F.B. Tett, and A.J. Weaver, 2004: Testing the linearity of the response to combined greenhouse gas and sulfate aerosol forcing. *Geophys. Res. Lett.,* **31**, L14201, DOI 10.1029/2004GL020111.

Gregory, J.M., W.J. Ingram, M.A. Palmer, G.S. Jones, P.A. Stott, R.B. Thorpe, J.A. Lowe, T.C. Johns, and K.D. Williams, 2004: A new method for diagnosing radiative forcing and climate sensitivity. *Geophysical Research Letters,* **31**(3), art. no.-L03205.

Hansen, J., Mki. Sato, R. Ruedy, L. Nazarenko, A. Lacis, G.A. Schmidt, G. Russell, I. Aleinov, M. Bauer, S. Bauer, N. Bell, B. Cairns, V. Canuto, M. Chandler, Y. Cheng, A. Del Genio, G. Faluvegi, E. Fleming, A. Friend, T. Hall, C. Jackman, M. Kelley, N. Kiang, D. Koch, J. Lean, J. Lerner, K. Lo, S. Menon, R.L. Miller, P. Minnis, T. Novakov,

V. Oinas, Ja. Perlwitz, Ju. Perlwitz, D. Rind, A. Romanou, D. Shindell, P. Stone, S. Sun, N. Tausnev, D. Thresher, B. Wielicki, T. Wong, M. Yao, and S. Zhang 2005. Efficacy of climate forcings. *J. Geophys. Res.* **110**, D18104, doi:10.1029/2005JD005776.

IPCC, 2000: *Emissions Scenarios. Special Report of the Intergovernmental Panel on Climate Change* [N. Nakicenovic, and R. Swart (eds.)]. Cambridge University Press, Cambridge, UK, 570 pp.

IPCC, 2001: *Climate Change 2001: The Scientific Basis. Contribution of Working Group I to the Third Assessment Report of the Intergovernmental Panel on Climate Change (IPCC)* [J.T. Houghton, Y. Ding, D.J. Griggs, M. Noguer, P.J. van der Linden, X. Dai, K. Maskell, and C.A. Johnson (eds.)]. Cambridge University Press, Cambridge, UK, 881 pp.

Joshi, M., K. Shine, M. Ponater, N. Stuber, R. Sausen, and L. Li, 2003: A comparison of climate response to different radiative forcings in three general circulation models: towards an improved metric of climate change. *Clim. Dynam.,* 20, 843-854.

Matthews, H.D., A.J. Weaver, M. Eby, and K.J. Meissner, 2003: Radiative forcing of climate by historical land cover change. *Geophys. Res. Lett.,* **30**, 271-274.

Meehl, G.A., W.M. Washington, C.M. Ammann, J.M. Arblaster, T.M.L. Wigley, and C. Tebaldi, 2004: Combinations of Natural and Anthropogenic Forcings in Twentieth-Century Climate. J. Climate, 17, 3721-3727.

Santer, B.D., T.M.L. Wigley, C. Mears, F.J. Wentz, S.A. Klein, D.J. Seidel, K.E. Taylor, P.W. Thorne, M.F. Wehner, P.J. Gleckler, J.S. Boyle, W.D. Collins, K.W. Dixon, C. Doutriaux, M. Free, Q. Fu, J.E. Hansen, G.S. Jones, R. Ruedy, T.R. Karl, J.R. Lanzante, G.A. Meehl, V. Ramaswamy, G. Russell, and G.A. Schmidt 2005. Amplification of surface temperature trends and variability in the tropical atmosphere. *Science* **309**, 1551-1556, doi:10.1126/science.1114867.

Senior, C.A., and J.F.B. Mitchell, 2000: The time-dependence of climate sensitivity. *Geophysical Research Letters,* **27**(17), 2685-2688.

Shine, K.P., J. Cook, E.J. Highwood, and M.M. Joshi, 2003: An alternative to radiative forcing for estimating the relative importance of climate change mechanisms. *Geophysical Research Letters,* **30**(20), art. no.-2047.

Soden, B.J. and Held, I.M., 2006: An assessment of climate feedbacks in coupled ocean-atmosphere models. *J. Clim.*, in press.

Stephens, G. L., 2005: Clouds in the climate system: a critical review, *J. Clim*., 18, 237-273.

Figure captions

Figure 1. The OLS regression of Q-N vs. ΔT_s, used to diagnose the Y terms, is shown for two models, based on the first 70 years of data from their 1%/year CO_2 increase integrations. CGCM3.1(T47) (top) had one of the better constrained Y estimates. In contrast, the FGOALS-g1.0 model (bottom) had the least constrained estimate. Shown from left to right are Y-LW, Y-SW and Y-NET regressions. The titles of each plot show the derived Y value and its 1σ uncertainty range, as calculated by OLS regression.

Figure 2. The OLS regression of Q-N vs. ΔT_s, used to diagnose the Y terms, is shown for four models, based on 220 years of data from their 1%/year CO_2 increase integration. In these simulations CO_2 is held constant after year 70 when CO_2 concentration reaches twice its initial value. Shown from left to right are Y-LW, Y-SW and Y-NET regressions. The titles of each plot show the derived Y value and its 1σ uncertainty range, as calculated by OLS regression. The first three rows are models that exhibited non-linearities in their derived values. The CCSM3 model shown in the fourth row is illustrative of the majority of models which did not exhibit marked non-linearities.

Figure 3: a) Y-LW and Y-SW values and b) Y-LW and Y-NET values derived from the 1%/year CO_2 increase model integrations. Shown as horizontal and vertical lines centered on each model estimate are 1σ uncertainty ranges from OLS regression. Estimates based on observations are shown in black (from the work of Forster and Gregory, 2006); these estimates have errors that extend beyond the plot boundaries.

Figure 4. Black lines show time series from 1850-2000 of diagnosed shortwave and longwave climate forcing relative to the pre-industrial control simulation. Results from

twenty climate models and the Myhre et al. (2001) estimate are shown. Preindustrial values are ~1850 for most models and 1750 for Myhre et al. (2001). The model name refers to the time series below it. Each of the time series begins near the corresponding zero line, and tick intervals are $1 Wm^{-2}$. The solar constant component, which is included in the plotted total shortwave climate forcing, is also shown separately as the blue line on the left panel. For four models independent estimates of the radiative forcing are shown as the magenta lines.

Figure 5. Black lines show time series of diagnosed shortwave and longwave climate forcing for the 21st Century SRESA1B scenario. Results from twenty climate models and an IPCC (2001) estimate based on SRESA1B tables are also shown. The model name refers to the time series below it. Each of the time series begins near the corresponding zero line, and tick intervals are $1 Wm^{-2}$. The solar constant component, which is included in the plotted shortwave climate forcing, is also shown separately as the blue line on the left panel. Data in these time series have been smoothed with a 10-year running mean filter. The magenta lines show the statistical error in the climate forcing diagnostic. These forcing time series are derived using the 1σ statistical uncertainty values of Y-SW and Y-LW in Equation 1.

Figure 6. Changes in the longwave and shortwave climate forcing calculated from the twenty models and from Myhre et al. (2001) or IPCC (2001), indicated by triangles. These forcing changes over 50 or 100 years are differences between two 9-year averages centered on the start and end years given in the panel titles.

Tables

Table 1. The models used in this paper and the summary of their included radiative forcings (indicated by a "Y"), following Santer et al. (2005). Further model details can be found at http://www-pcmdi.llnl.gov/ipcc/model_documentation/ipcc_model_documentation.php.

AOGCM	G	O	SD	SI	BC	OC	MD	SS	LU	SO	VL
CGCM3.1 (T47 and T63)	Y	-	Y	-	-	-	-	-	-	-	-
CNRM-CM3	Y	Y	Y	-	Y	-	-	-	-	-	-
CSIRO-Mk3	Y	-	Y	-	?	?	?	?	?	?	-
GFDL-CM2.0	Y	Y	Y	-	Y	Y	-	-	Y	Y	Y
GFDL-CM2.1	Y	Y	Y	-	Y	Y	-	-	Y	Y	Y
GISS-EH	Y	Y	Y	Y	Y	Y	Y	Y	Y	Y	Y
GISS-ER	Y	Y	Y	Y	Y	Y	Y	Y	Y	Y	Y
FGOALS-g1.0	Y	-	Y	?	-	-	-	-	-	-	-
IPSL-CM4	Y	-	Y	Y	-	-	-	-	-	-	-
MIROC3.2(hires)	Y	Y	Y	?	Y	Y	Y	Y	Y	Y	Y
MIROC3.2(medres)	Y	Y	Y	?	Y	Y	Y	Y	Y	Y	Y
ECHO-G	Y	-	Y	Y	-	-	-	-	-	Y	Y*
ECHAM5	Y	Y	Y	Y	-	-	-	-	-	-	-
MRI-CGCM2.3.2	Y	-	Y	-	-	-	-	-	-	Y	Y*
CCSM3	Y	Y	Y	-	Y	Y	-	-	-	Y	Y
HadCM3	Y	Y	Y	Y	-	-	-	-	-	-	-
HadGEM1	Y	Y	Y	Y	Y	Y	-	-	Y	Y	Y
INM-CM3.0	Y	-	Y	-	-	-	-	-	-	Y	-
PCM1	Y	Y	Y	-	-	-	-	-	-	Y	Y

G = Well-mixed greenhouse gases
O = Tropospheric and stratospheric ozone
SD = Sulfate aerosol direct effects
SI = Sulfate aerosol indirect effects
BC = Black carbon
OC = Organic carbon
MD = Mineral dust
SS = Sea salt
LU = Land use change
SO = Solar irradiance
VL = Volcanic aerosols

Y*: Volcanic aerosols modeled as a solar constant change

Table 2. The $2xCO_2$ radiative forcings computed by the AOGCM groups. Longwave adjusted all-sky (LW, ADJ) and instantaneous clear sky (LW, CLR-INST) are shown, where "adjusted" refers to forcing calculated after stratospheric adjustment. The shortwave instantaneous all-sky forcing (SW, INST) and NET adjusted forcing (NET, ADJ) are also shown. The Myhre *et al.* (1998) values are from a reference line-by-line model. These reference RF values are assumed for AOGCMs which do not diagnose their own RF values (see text).

AOGCM	**LW**		**SW**	**NET**
	ADJ	**CLR-INST**	**INST**	**ADJ**
	(Wm^{-2})			
CGCM3.1(T47)	3.39	-	-	3.39
GISS-EH	4.21	5.17	-0.15	4.06
IPSL-CM4	3.50	-	-	3.50
MIROC3.2(hires)	3.59	4.59	0.00	3.59
MIROC3.2(medres)	3.66	4.56	0.00	3.66
ECHAM5	3.98	4.94	0.03	4.01
CCSM3	4.23	4.89	-0.28	3.95
HadCM3	4.03	5.13	-0.22	3.80
HadGEM1	4.02	5.22	-0.24	3.78
AOGCM Average	**3.85**	**4.93**	**-0.12**	**3.75**
STD-dev	**0.31**	**0.27**	**0.13**	**0.23**
Myhre et al. 1998	**3.85**	**4.94**	**-0.15**	**3.70**

Table 3. In the first block of numbers AOGCM results are given for the diagnosed climate feedback (*Y*) terms and the 1 standard deviation uncertainties (see Section 5). Note that all but the last column of values in this block come from the 1% per year CO_2 increase integrations. The values in the last column of this block come from doubled CO_2 equilibrium experiments performed with atmospheric models coupled to slab-oceans. For these calculations $2xCO_2$ radiative forcing estimates are taken from Table 2. The next block contains the diagnosed climate forcing values (*Q*) for year 2100 relative to preindustrial times (see Section 6) obtained from the SRESA1b simulations. Values in the right-most column are the globally averaged surface temperature changes at year 2100 relative to preindustrial times (see Section 7). For comparison the last row in the table presents forcing values for the SRESA1B scenario presented in IPCC (2001).

AOGCM	YLW	1σ	YSW	1σ	YNET	1σ	YNET $2xCO_2$	QLW 2100	QSW 2100	QNET 2100	ΔT_s 2100
	($Wm^{-2}K^{-1}$)							(Wm^{-2})			(K)
CGCM3.1(T47)	2.48	0.15	-1.34	0.16	1.14	0.17	1.02	6.30	-0.79	5.51	3.65
CGCM3.1(T63)	2.22	0.11	-1.20	0.11	1.02	0.11	1.09	5.86	-0.36	5.50	4.33
CNRM-CM3	3.14	0.22	-1.63	0.24	1.51	0.26		8.62	-0.85	7.77	4.04
CSIRO-Mk3	2.81	0.26	-1.22	0.12	1.58	0.29	1.23	6.77	-0.69	6.07	2.83
GFDL-CM2.0	2.48	0.22	-0.85	0.15	1.63	0.21		6.73	0.03	6.75	3.30
GFDL-CM2.1	2.22	0.24	-0.46	0.17	1.76	0.24		6.68	0.15	6.83	3.03
GISS-EH	2.32	0.18	-0.67	0.11	1.65	0.18	1.54	7.67	-2.27	5.40	2.54
GISS-ER	2.44	0.16	-0.77	0.10	1.67	0.17		7.67	-1.80	5.87	2.48
FGOALS-g1.0	1.94	0.28	-0.07	0.08	1.87	0.35		7.24	0.67	7.91	3.59
INM-CM3.0	1.78	0.24	-0.20	0.10	1.58	0.28	1.83	5.72	0.16	5.88	3.07
IPSL-CM4	2.67	0.35	-1.75	0.21	0.92	0.17		6.41	-0.56	5.86	3.94
MIROC3.2(hires)	2.53	0.15	-1.63	0.15	0.91	0.14	0.88	7.07	-0.82	6.25	4.88
MIROC3.2(medres)	2.47	0.15	-1.49	0.16	0.98	0.17	0.92	6.45	-0.77	5.69	3.76
ECHO-G	1.65	0.20	-0.18	0.06	1.48	0.19		6.88	-0.93	5.95	3.55
ECHAM5	2.04	0.18	-0.92	0.18	1.12	0.17	1.24	6.64	-1.01	5.64	3.60
MRI-CGCM2.3.2	1.80	0.22	-0.57	0.12	1.23	0.16		4.23	0.40	4.62	2.97
CCSM3	2.51	0.20	-0.65	0.09	1.86	0.27	1.48	7.66	-0.18	7.48	3.22
PCM1	1.91	0.30	-0.10	0.05	1.81	0.28		5.28	0.20	5.48	2.54
HadCM3	2.28	0.19	-1.02	0.17	1.26	0.19	1.07	7.52	-1.46	6.06	3.61
HadGEM1	2.43	0.14	-1.05	0.16	1.38	0.21	0.93	7.48	-0.17	7.31	3.91
AOGCM AVG.	**2.31**		**-0.89**		**1.42**		**1.20**	**6.74**	**-0.55**	**6.19**	**3.44**
AOGCM StdDev	**0.37**		**0.53**		**0.32**		**0.30**	**0.98**	**0.75**	**0.88**	**0.63**
IPCC SRESA1B								**6.75**	**-0.23**	**6.52**	

Figures

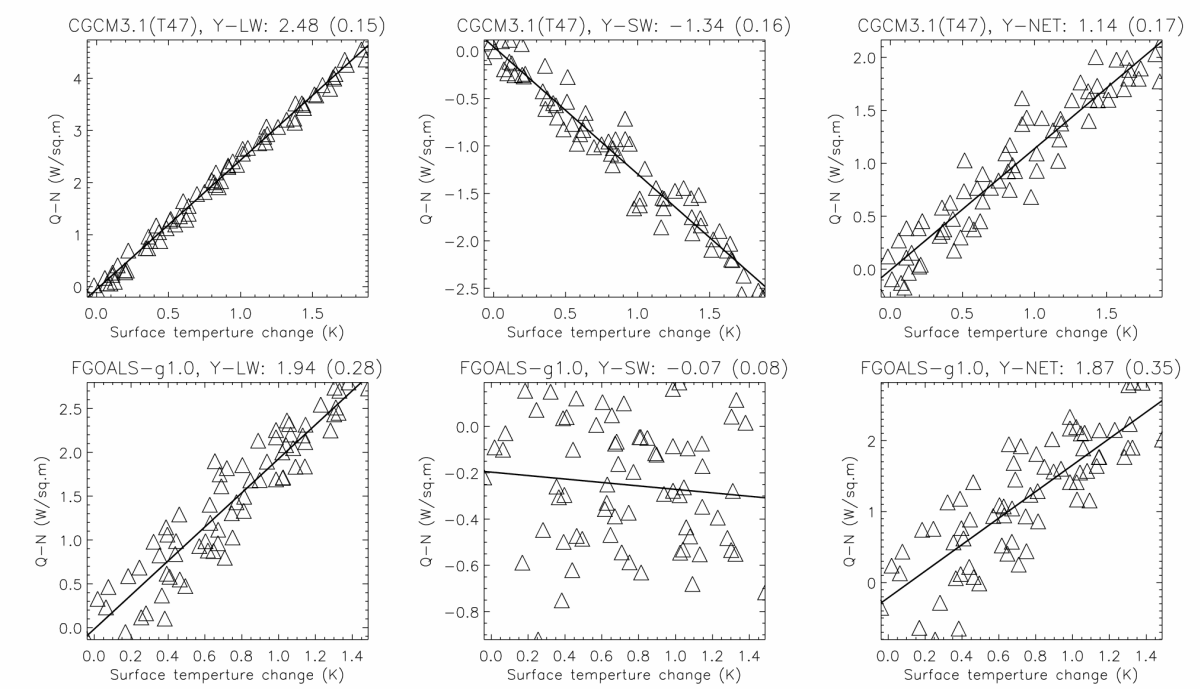

Figure 1. The OLS regression of Q-N vs. ΔT_s, used to diagnose the Y terms, is shown for two models, based on the first 70 years of data from their 1%/year CO_2 increase integrations. CGCM3.1(T47) (top) had one of the better constrained Y estimates. In contrast, the FGOALS-g1.0 model (bottom) had the least constrained estimate. Shown from left to right are Y-LW, Y-SW and Y-NET regressions. The titles of each plot show the derived Y value and its 1σ uncertainty range, as calculated by OLS regression.

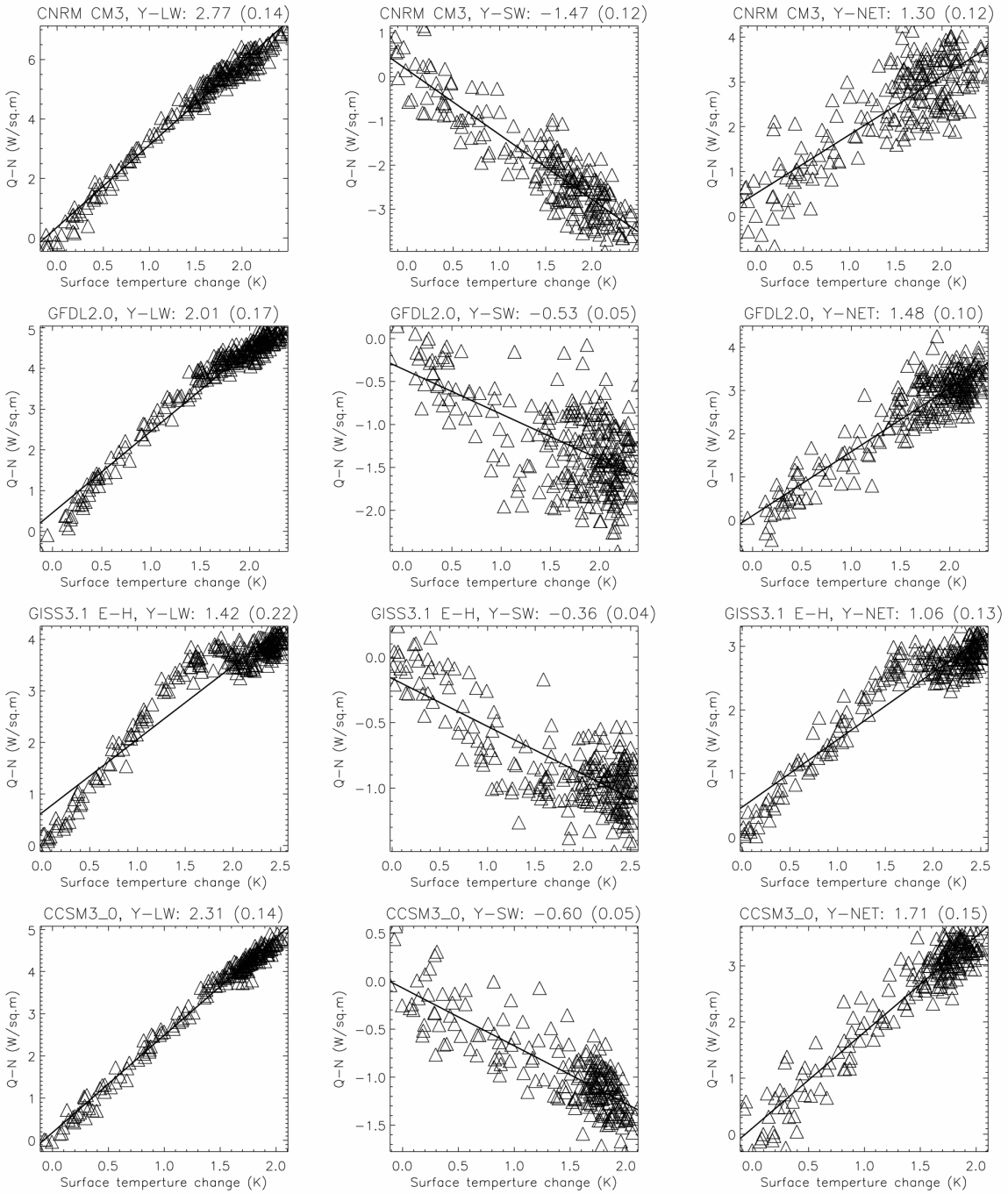

Figure 2. The OLS regression of Q-N vs. ΔT_s, used to diagnose the Y terms, is shown for four models, based on 220 years of data from their 1%/year CO_2 increase integration. In these simulations CO_2 is held constant after year 70 when CO_2 concentration reaches twice its initial value. Shown from left to right are Y-LW, Y-SW and Y-NET regressions. The titles of each plot show the derived Y value and its 1σ uncertainty range, as

calculated by OLS regression. The first three rows are models that exhibited non-linearities in their derived values. The CCSM3 model shown in the fourth row is illustrative of the majority of models which did not exhibit marked non-linearities.

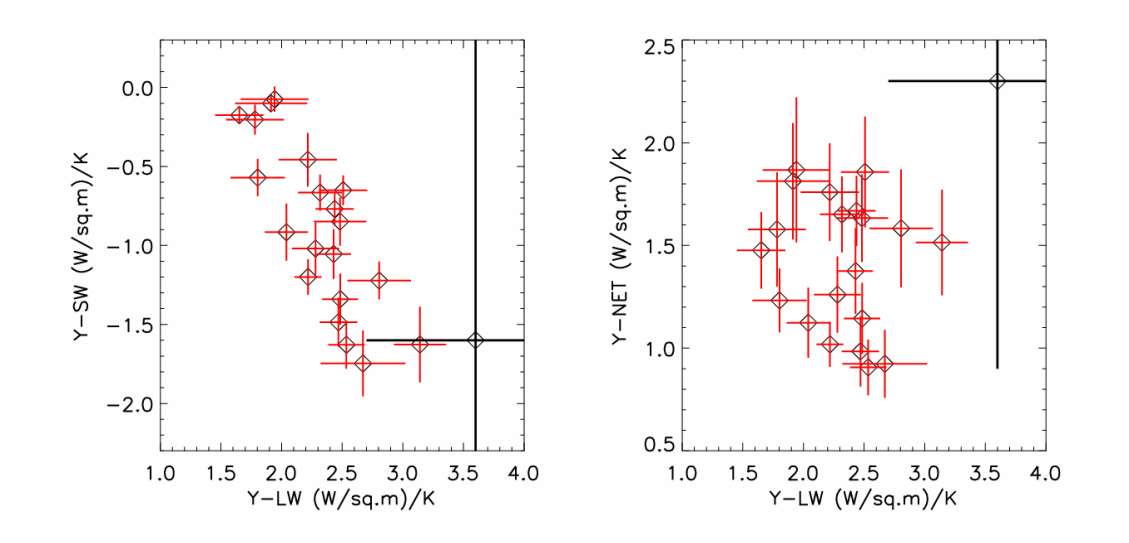

Figure 3: a) Y-LW and Y-SW values and b) Y-LW and Y-NET values derived from the 1%/year CO_2 increase model integrations. Shown as horizontal and vertical lines centered on each model estimate are 1σ uncertainty ranges from OLS regression. Estimates based on observations are shown in black (from the work of Forster and Gregory, 2006); these estimates have errors that extend beyond the plot boundaries.

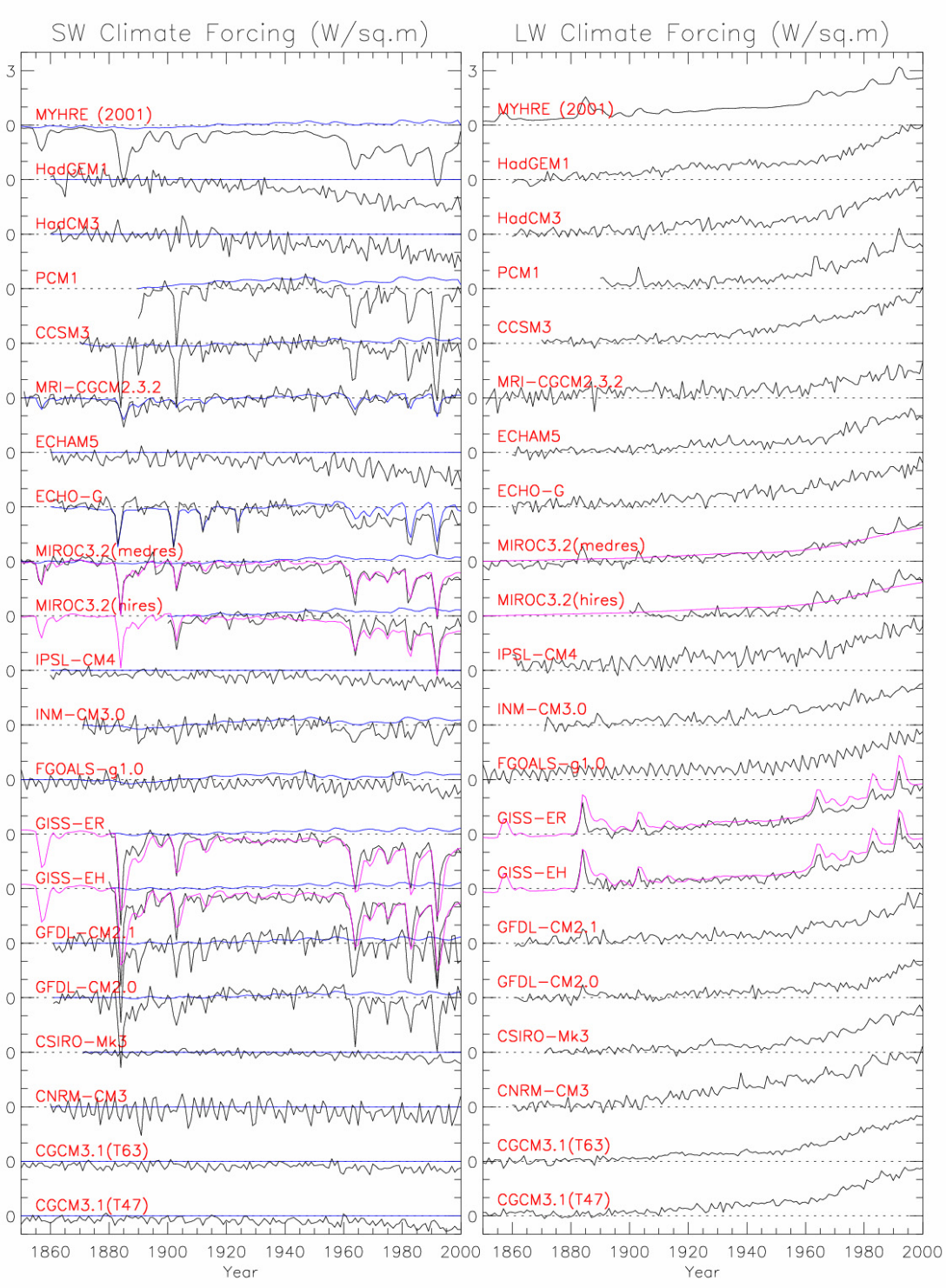

Figure 4. Black lines show time series from 1850-2000 of diagnosed shortwave and longwave climate forcing relative to the pre-industrial control simulation. Results from twenty climate models and the Myhre et al. (2001) estimate are shown. Preindustrial values are ~1850 for most models and 1750 for Myhre et al. (2001). The model name

refers to the time series below it. Each of the time series begins near the corresponding zero line, and tick intervals are $1 Wm^{-2}$. The solar constant component, which is included in the plotted total shortwave climate forcing, is also shown separately as the blue line on the left panel. For four models independent estimates of the radiative forcing are shown as the magenta lines.

Figure 5. Black lines show time series of diagnosed shortwave and longwave climate forcing for the 21st Century SRESA1B scenario. Results from twenty climate models and an IPCC (2001) estimate based on SRESA1B tables are also shown. The model name refers to the time series below it. Each of the time series begins near the corresponding zero line, and tick intervals are $1 Wm^{-2}$. The solar constant component, which is included

in the plotted shortwave climate forcing, is also shown separately as the blue line on the left panel. Data in these time series have been smoothed with a 10-year running mean filter. The magenta lines show the statistical error in the climate forcing diagnostic. These forcing time series are derived using the 1σ statistical uncertainty values of Y-SW and Y-LW in Equation 1.

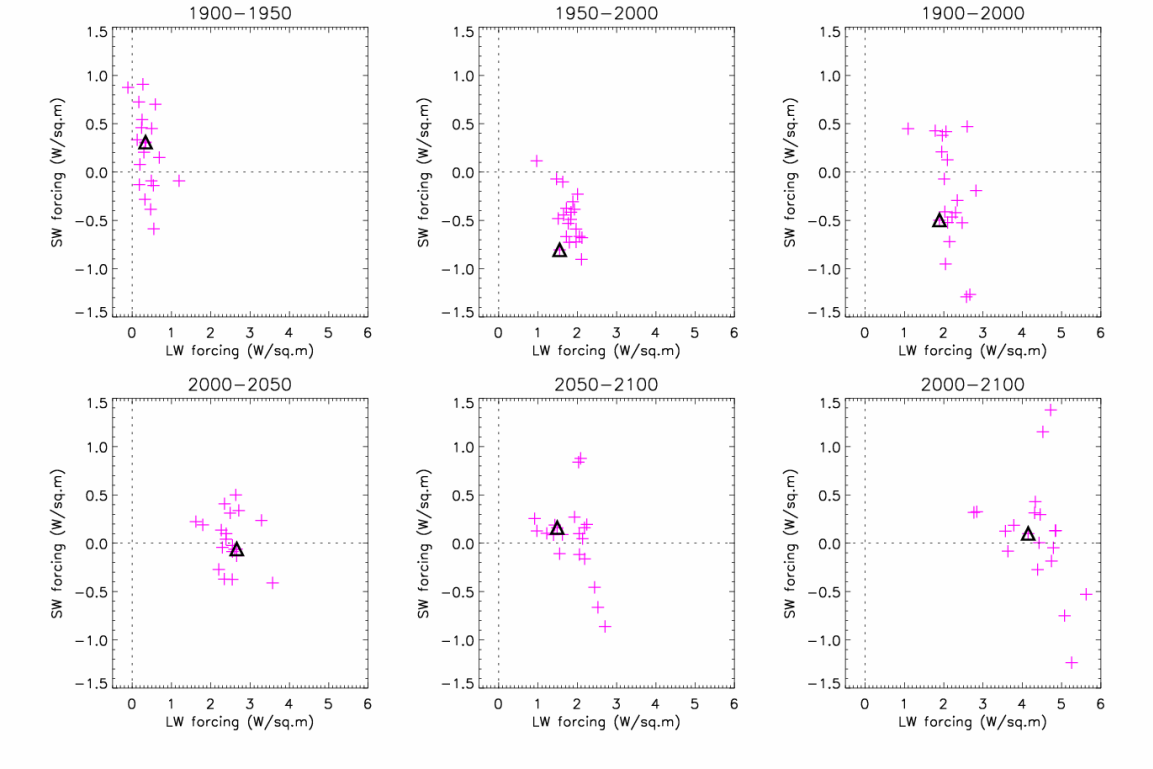

Figure 6. Changes in the longwave and shortwave climate forcing calculated from the twenty models and from Myhre et al. (2001) or IPCC (2001), indicated by triangles. These forcing changes over 50 or 100 years are differences between two 9-year averages centered on the start and end years given in the panel titles.